



Synthetic aperture controlled source electromagnetics

Y. Fan,¹ R. Snieder,¹ E. Slob,^{1,2} J. Hunziker,² J. Singer,³ J. Sheiman,³ and M. Rosenquist³

Received 13 May 2010; accepted 7 June 2010; published 9 July 2010.

[1] Controlled-source electromagnetics (CSEM) has been used as a de-risking tool in the hydrocarbon exploration industry. Although there have been successful applications of CSEM, this technique is still not widely used in the industry because the limited types of hydrocarbon reservoirs CSEM can detect. In this paper, we apply the concept of synthetic aperture to CSEM data. Synthetic aperture allows us to design sources with specific radiation patterns for different purposes. The ability to detect reservoirs is dramatically increased after forming an appropriate synthetic aperture antenna. Consequently, the types of hydrocarbon reservoirs that CSEM can detect are significantly extended. Because synthetic apertures are constructed as a data processing step, there is no additional cost for the CSEM acquisition. Synthetic aperture has potential for simplifying and reducing the cost of CSEM acquisition. We show a data example that illustrates the increased sensitivity obtained by applying synthetic aperture CSEM source. **Citation:** Fan, Y., R. Snieder, E. Slob, J. Hunziker, J. Singer, J. Sheiman, and M. Rosenquist (2010), Synthetic aperture controlled source electromagnetics, *Geophys. Res. Lett.*, 37, L13305, doi:10.1029/2010GL043981.

1. Introduction

[2] After the development in academia starting in the late 1970s [Spiess *et al.*, 1980; Cox, 1981; Young and Cox, 1981] and the early industry experiments [Srnska, 1986; Constable *et al.*, 1986; Chave *et al.*, 1991; Hoversten and Unsworth, 1994], CSEM was introduced to the industry at the beginning of this century as a method to explore hydrocarbons. Since then the research and commercial surveys on CSEM have boomed [Constable and Srnska, 2007; Chopra *et al.*, 2007].

[3] The fundamental concept and the assumption of using CSEM as a detector of hydrocarbons is that porous rocks are resistive when they are saturated with gas or oil [Edwards, 2005; Constable and Srnska, 2007]. In a standard CSEM survey, a horizontal current dipole is used as the source to generate an electromagnetic field and is towed close to the sea floor to avoid energy loss in the conductive sea water. The receivers are located on the sea floor. A resistive hydrocarbon reservoir in the subsurface (a target with a resistivity of approximate 50 to 100 Ωm) embedded in the conductive background (about 1 Ωm), acts as a secondary

source that directs the electromagnetic field back to the receivers. In this way, one can infer the presence of a resistive body in the subsurface from the measured electromagnetic field.

[4] The main challenge in CSEM is the diffusive nature of the electromagnetic field in the conductive subsurface. Thus the secondary field that refracts from the target is much smaller at most offsets than the field which does not carry any information of the subsurface, such as the direct arrival and the air wave, [Edwards, 2005; Constable and Srnska, 2007].

[5] We introduce the concept of synthetic aperture to CSEM data. Synthetic aperture allows us to design sources with specific radiation patterns for different purposes. Here we construct a synthetic aperture antenna to steer the electromagnetic field into a designed direction. By doing this, one can concentrate the energy toward the target. At the same time, the background field (e.g., air wave) is significantly reduced. Consequently, the ability to detect the reservoirs is dramatically increased after forming appropriate synthetic apertures without any increase in acquisition cost.

2. Synthetic Aperture Method for Diffusion

[6] Although synthetic aperture has been a widely used concept for waves such as radar and sonar [Barber, 1985; Ralston *et al.*, 2007; Zhou *et al.*, 2009; Cutrona, 1975; Riyait *et al.*, 1995; Bellettini and Pinto, 2002], to the best of the authors' knowledge, this is the first time that synthetic aperture has been introduced to a diffusive field as used in CSEM. The basic idea of synthetic aperture is to use the interference of fields radiated by different sources to construct a virtual source with a specific radiation pattern. One fundamental question is: can one apply wave-based concepts to a diffusive field? Although waves and diffusion behave differently in the time domain, their expressions are similar in the frequency domain. For example the 3D diffusion equation in an homogeneous medium can be written in the frequency domain as

$$D\nabla^2 G(\mathbf{r}, \mathbf{r}_s, \omega) - i\omega G(\mathbf{r}, \mathbf{r}_s, \omega) = -\delta(\mathbf{r} - \mathbf{r}_s), \quad (1)$$

where D is the diffusivity of the medium, δ the Dirac-Delta function, ω the angular frequency, and $G(\mathbf{r}, \mathbf{r}_s, \omega)$ the Green's function at position \mathbf{r} from a source at \mathbf{r}_s . The homogeneous equation $D\nabla^2 u(\mathbf{r}, \omega) - i\omega u(\mathbf{r}, \omega) = 0$ has plane wave solution in the frequency domain

$$u(\mathbf{r}, \omega) = e^{-i\alpha\hat{\mathbf{n}}\cdot\mathbf{r}} e^{-\alpha\hat{\mathbf{n}}\cdot\mathbf{r}}, \quad (2)$$

where $\alpha = \sqrt{\omega/(2D)}$. Equation (2) shows that at a single angular frequency ω , diffusion can be treated as damped waves [Mandelis, 2000]. Term $e^{-i\alpha\hat{\mathbf{n}}\cdot\mathbf{r}}$ defines the propagation of the field in the $\hat{\mathbf{n}}$ direction and $e^{-\alpha\hat{\mathbf{n}}\cdot\mathbf{r}}$ defines the

¹Center for Wave Phenomena, Colorado School of Mines, Golden, Colorado, USA.

²Section of Applied Geophysics and Petrophysics, Department of Geotechnology, Delft University of Technology, Delft, Netherlands.

³Shell International Exploration and Production, Houston, Texas, USA.

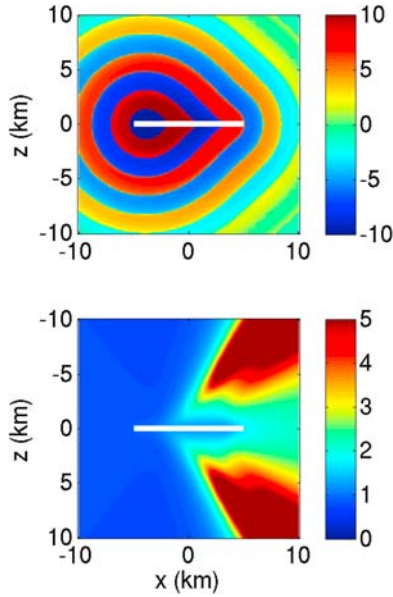


Figure 1. (top) The imaginary part of the field after steering with the color map in \log_{10} scale. (bottom) Ratio of the field amplitude with steering to the amplitude without steering. The white bar in Figures 1 (top) and 1 (bottom) illustrates the size of the synthetic aperture.

decay of the field in the \hat{n} direction. Note that like waves at a single frequency, diffusion also admits solutions with a specific direction of propagation. From equation (2), one can calculate the wavelength, phase velocity, amplitude and phase at any given point [Yodh and Chance, 1995]. In fact, the interference of diffusion-waves (diffusive field from an oscillatory source [Mandelis, 2000]) has been studied in physics [Schmitt et al., 1992, 1993; Knuttel et al., 1993; Yodh and Chance, 1995; Wang and Mandelis, 1999]. Therefore, it is logical to apply the synthetic aperture concept to diffusive fields in the frequency domain. Since in the current CSEM the field is analyzed in the frequency domain, we further apply the synthetic aperture concept in CSEM.

[7] A general formula for constructing a synthetic aperture S_A is

$$S_A(\mathbf{r}, \omega) = \sum_{n=1}^N a_n e^{i\phi_n} s(\mathbf{r}, \mathbf{r}_n, \omega). \quad (3)$$

At a single angular frequency ω , a synthetic source at location r is a superposition of the sequentially distributed sources that are located from \mathbf{r}_1 to \mathbf{r}_N with an amplitude weighting a_n and a phase shift ϕ_n .

[8] We show an example of a 10 km synthetic aperture with field steering using the Green's function $G(\mathbf{r}, \mathbf{r}_s, \omega) = \frac{1}{4\pi D|\mathbf{r}-\mathbf{r}_s|} e^{-i\alpha|\mathbf{r}-\mathbf{r}_s|} e^{-\alpha|\mathbf{r}-\mathbf{r}_s|}$ for equation (1) [Mandelis, 2001]. We use the diffusivity of electromagnetic field in sea water $2.4 \times 10^5 \text{ m}^{-1}$ ($D = 1/(\mu\sigma)$, where μ is the permeability and σ is the conductivity). The frequency used in this example is 0.25 Hz. The Green's function from the synthetic aperture is defined as

$$G_A(\mathbf{r}) = \int_{-5km}^{5km} e^{-ic_1\alpha\Delta x} e^{-c_2\alpha\Delta x} G(\mathbf{r}, x, \omega) dx. \quad (4)$$

where c_1 is a coefficient to control the steering angle, c_2 is a coefficient to compensate the energy loss due to the diffusion, and $\Delta x = |x + 5| \text{ km}$ is the distance between each source and the left edge of the aperture. In this particular example we use $c_1 = 0.7$, which corresponds to a steering angle of $\theta = \pi/4$ (angle between the steering direction and vertical axis). The steering angle is related to c_1 by $c_1 = \sin\theta$. The coefficient c_2 is set to be the same as c_1 because the coefficient α corresponding the field decay is the same as that for phase in equation (2). Figure 1 (top) shows $\text{sign}(ImG_A) \log_{10}|ImG_A|$, which is the logarithm of $|ImG_A|$ with a minus sign when ImG_A is negative. The white bar in the center of Figure 1 shows to the size of the synthetic aperture. Figure 1 (bottom) is the ratio of the field amplitude with a phase steering to the field amplitude without the phase steering, defined as

$$R = \frac{\left| \int_{-5km}^{5km} e^{-ic_1\alpha\Delta x} e^{-c_2\alpha\Delta x} G(\mathbf{r}, x, \omega) dx \right|}{\left| \int_{-5km}^{5km} e^{-c_2\alpha\Delta x} G(\mathbf{r}, x, \omega) dx \right|}. \quad (5)$$

This ratio is the largest at angle $\pi/4$ from the synthetic aperture. This example illustrates that we can indeed steer a diffusive field to a designed angle. Although we only show the field steering aspect of synthetic aperture in this paper, general synthetic aperture concepts can be applied much widely. For example, a quadratic phase shift applied to the source signal can, in principle, be use to focus the field.

3. Synthetic and Field Data Example

3.1. Synthetic Data Example

[9] In the numerical model shown next we use a hydrocarbon reservoir (centered at the origin with horizontal extent of 5 km in the x and y directions and a thickness of 100 m) located 1 km below the sea floor. The sea water is 1 km deep with a resistivity of 0.3 Ωm . The subsurface background is a half space with a resistivity of 1 Ωm . The resistivity of the reservoir is set to be 100 Ωm . The receivers are located at the sea floor and a 100 m dipole source with a current of 100 A is continuously towed 100 m above the receivers. The source current oscillates with a frequency of 0.25 Hz. All the analysis in this research are in the frequency domain using 0.25 Hz data.

[10] In this example, we focus on the construction of a synthetic aperture source with the field steered toward the target direction. Figure 2a shows the inline electrical fields with the reservoir (dashed line) and without the reservoir (solid line) from a single 100 m dipole whose center is located at $x = -6.5 \text{ km}$. There is a slight increase in the field around the position $x = 0 \text{ km}$ when the reservoir is present. This 20% difference is shown by the ratio of the field with the reservoir to the field without the reservoir (black solid curve in Figure 2e).

[11] Simply superposing the 50 employed sequential sources, is equivalent to setting $a_n = 1$, $\phi_n = 0$, and $N = 50$ in equation (3). This superposition gives a 5 km long dipole source with a current of 100 A. The total E_x field is given by Figure 2b. The ratio of the fields with and without the reservoir is shown by the red dashed curve in Figure 2e. Although the overall signal strength increases compared to

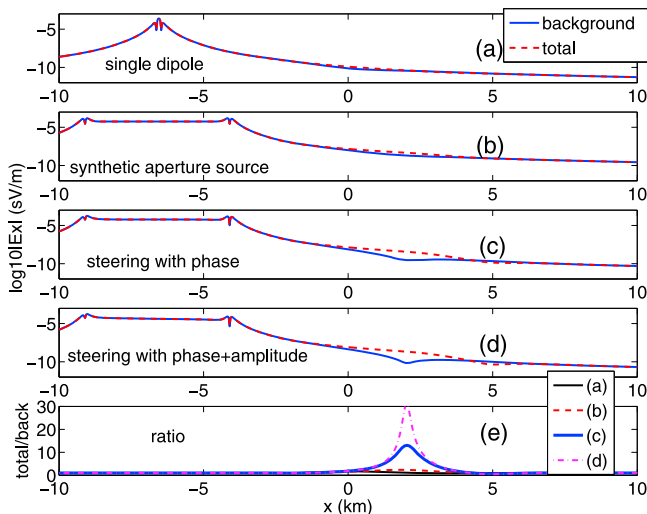


Figure 2. Inline electrical fields with the reservoir (dashed lines) and without the reservoir (solid) for four different sources; (a) a 100 m dipole source; (b) a 5 km dipole source; (c) a 5 km synthetic source obtained from field steering toward the target by the phase shift; (d) a 5 km synthetic source obtained from field steering toward the target by the phase shift and the amplitude compensation. (e) The ratio between the fields with and without the reservoir. The four curves in Figure 2e represent the ratios from Figures 2a–2d.

the single 100 m source (Figure 2a), the difference between the models with and without the reservoir does not significantly increase by simply using a longer dipole.

[12] Instead of using a zero phase shift in equation (3), we next apply a linear phase shift to the sequential sources using $\phi_n = c_1 n \Delta s$, with $c_1 = \sin \frac{\pi}{4}$ and where Δs is the distance between the centers of two neighboring sources and c_1 is defined in equation (4). As illustrated in Figure 1, this phase shift steers the total field toward the right. Figure 2c shows the E_x field excited by this new synthetic aperture source. The ratio of the steered fields is illustrated by the blue solid curve in Figure 2e. This example shows that the detectability of the reservoir significantly increases by steering the field toward the target.

[13] There are two reasons for the improved detectability. First, the total electrical field as well as the z component of the E field increases at the target location when the field propagation is steered from the vertical direction to a tilted angle. The z component of the E field diagnoses changes in the conductivity in the vertical direction [Edwards, 2005]. Second, a comparison of Figures 2b and 2c shows that the background field (solid lines) on the right side of the source is reduced by the field steering.

[14] The attenuation of a diffusive field, causes the sources on the left side to give a smaller contribution to the synthetic aperture construction because they propagate a greater distance. In order to have a more effective steered field, we use an energy compensation term $a_n = e^{-c_2 n \Delta s}$ as we used in equation (4), where c_2 is a constant that controls the amplitude weighting. Although we used $c_2 = c_1$ in the homogeneous medium shown in equation (4), in this layered model the anomaly due to the reservoir is largest when c_2 is 0.1 m^{-1} . The optimization of c_1 and c_2 will be further

investigated and presented in a more detailed paper. After we include this energy compensation, the difference between the models with and without the target further increases, as shown in Figure 2d. This difference is quantified by the ratio of the fields with and without the target and is illustrated by the magenta dashed-dotted line in Figure 2e.

[15] The examples show that the synthetic aperture technique dramatically increases the difference in electrical field response between the models with and without the reservoir by a factor of 30. Note that this is achieved without altering the data acquisition. If noise is added in the above example, the main observation still holds, but in that case we can not steer the field as effective as for noise free data and therefore the anomaly ratio is not as big as the factor of 30.

3.2. Real Data Example

[16] Next, we apply field steering to the real data. In the real data, the field ‘without’ the target is defined as the measured field at a reference site under which there is no reservoir. For a standard single dipole measurement, the inline electrical fields with and without the reservoir are shown by the red dashed and black solid curves, respectively, in Figure 3a. The corresponding ratio of the two fields is shown by the solid curve in Figure 3d. Note that only the area between $x = 4 \text{ km}$ to $x = 15 \text{ km}$, where the reservoir imprint locates, is shown in Figure 3d. The reservoir is known to be located between $x = 3 \text{ km}$ and $x = 6 \text{ km}$. A slight difference in the electrical field, caused by the reservoir, can be observed between the offset of 6 km and 10 km. Beyond the offset of 10 km, the ratio oscillates because the field reaches the noise level.

[17] Next, we construct a 4 km synthetic aperture source with no field steering (zero phase shift). The fields with and without the reservoir are shown by the red dashed and black solid curves in Figure 3b, respectively, and the corresponding ratio is the red dashed curve in Figure 3d. Because the longer dipole source has a better signal to noise ratio (the

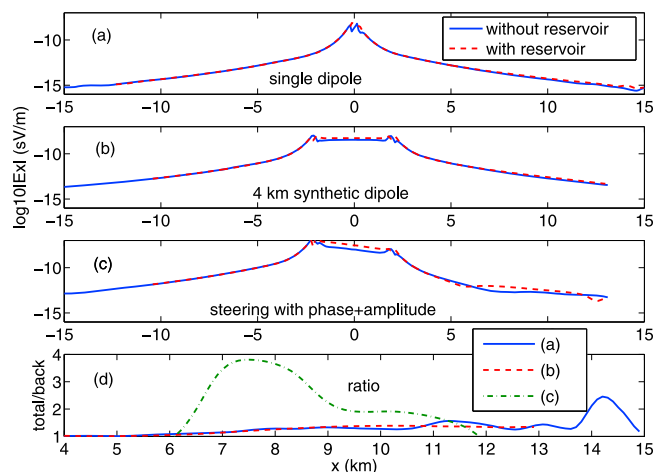


Figure 3. Inline electrical field with the reservoir (red dashed lines) and without the reservoir (black solid lines) for three different sources; (a) a single dipole source; (b) a 4 km synthetic source; (c) a 4 km synthetic source obtained from field steering toward the reservoir by the phase shift and the amplitude compensation. (d) The ratio between the fields with and without the reservoir. The three curves in Figure 3d represent the ratios from Figures 3a–3c.

signal is stronger), both the E_x field and the ratio are smoother than the field generated by an individual source. The overall difference between the responses, however, does not change too much.

[18] We next construct a 4 km synthetic aperture source with field steering toward the reservoir using a phase shift ($c_1 = 0.8$) and amplitude weighting ($c_2 = 0.6$). Figure 3c shows that the difference in the field between with and without the reservoir has significantly increased after we apply the field steering. The corresponding ratio is shown by green dashed-dotted line in Figure 3d. The imprint of the reservoir is much more pronounced in Figure 3c than those in Figures 3a and 3b. Note that the response at negative offsets does not show any difference in the field both before and after the field steering. This is because there is no reservoir for negative offsets.

4. Discussion and Conclusion

[19] The synthetic aperture technique opens a new line of research in CSEM data processing. Hidden information in CSEM data can be retrieved by using the synthetic aperture technique with no extra cost because there is no need to change the acquisition. The ability to detect reservoirs is dramatically increased after forming appropriate synthetic aperture sources. The depth of the reservoir that CSEM detects can potentially increase with the use of synthetic aperture methods. Additionally, synthetic aperture has potential for towing the source at shallower depth in the water, which would simplify CSEM acquisition and reduces the acquisition cost. In this paper, we only show examples of constructing synthetic aperture source in a line. In principle, one can construct 2D synthetic aperture surface source to better detect the 3D structure of the subsurface. For example, when data are collected with antennas along parallel lines, one not only can steer the field in the inline direction, but also in the crossline direction. The synthetic aperture technique is not limited to the source side, but can also be applied to the receiver side.

[20] **Acknowledgments.** The authors give special thanks to a reviewer and the editor for their constructive comments. We are grateful for the financial support from the Shell Gamechanger Project. The electromagnetic research team in Shell provided technical support in the research and we thank their permission for using the real data.

References

Barber, B. C. (1985), Theory of digital imaging from orbital synthetic-aperture radar, *Int. J. Remote Sens.*, *6*, 1009–1057.

- Belletini, A., and M. Pinto (2002), Theoretical accuracy of synthetic aperture sonar microneavigation using a displaced phase-center antenna, *IEEE J. Oceanic Eng.*, *27*, 780–789.
- Chave, A. D., S. C. Constable, and R. N. Edwards (1991), Electrical exploration methods for the seafloor, in *Electromagnetic Methods in Applied Geophysics*, vol. 2, edited by M. Nabighian, 931–966, Soc. of Explor. Geophys., Tulsa, Okla.
- Chopra, S., K. Strack, C. Esmersoy, and N. Allegar (2007), Introduction to this special section: CSEM, *Leading Edge*, *26*, 323–325.
- Constable, S., and L. J. Srnka (2007), An introduction to marine controlled-source electromagnetic methods for hydrocarbon exploration, *Geophysics*, *72*, WA3–WA12.
- Constable, S. C., C. S. Cox, and A. D. Chave (1986), Offshore electromagnetic surveying techniques, *SEG Expanded Abstr.*, *5*, 81–82.
- Cox, C. S. (1981), On the electrical conductivity of the oceanic lithosphere, *Phys. Earth Planet. Inter.*, *25*, 196–201.
- Cutrona, L. (1975), Comparison of sonar system performance achievable using synthetic-aperture techniques with the performance achievable, *J. Acoust. Soc. Am.*, *58*, 336–348.
- Edwards, N. (2005), Marine controlled source electromagnetics: Principles, methodologies, future commercial applications, *Surv. Geophys.*, *26*, 675–700.
- Hoversten, G. M., and M. Unsworth (1994), Subsalt imaging via seaborne electromagnetics, *Offshore Technol. Conf.*, *26*, 231–240.
- Knuttel, A., J. Schmitt, R. Barnes, and J. Knutson (1993), Acousto-optic scanning and interfering photon density waves for precise localization of an absorbing (or fluorescent) body in a turbid medium, *Rev. Sci. Instrum.*, *64*, 638–644.
- Mandelis, A. (2000), Diffusion waves and their uses, *Phys. Today*, *53*, 29.
- Mandelis, A. (2001), *Diffusion-Wave Fields: Mathematical Methods and Green Functions*, 1st ed., Springer, New York.
- Ralston, T. S., D. L. Marks, C. P. Scott, and S. A. Boppart (2007), Interferometric synthetic aperture microscopy, *Nat. Phys.*, *3*, 129–134.
- Riyait, V., M. Lawlor, A. Adams, O. Hinton, and B. Sharif (1995), Real-time synthetic aperture sonar imaging using a parallel architecture, *IEEE Trans. Image Process.*, *4*, 1010–1019.
- Schmitt, J. M., A. Knuttel, and R. F. Bonner (1993), Measurement of optical properties of biological tissues by low-coherence reflectometry, *Appl. Opt.*, *32*, 6032–6042.
- Schmitt, J. M., A. Knuttel, and J. R. Knutson (1992), Interference of diffusive light waves, *J. Opt. Soc. Am.*, *9*, 1832–1843.
- Spieß, F. N., et al. (1980), East Pacific Rise: Hot springs and geophysical experiments, *Science*, *207*, 1421–1433.
- Srnka, L. J. (1986), Method and apparatus for offshore electromagnetic sounding utilizing wavelength effects to determine optimum source and detector positions, Patent 4,617,518, U.S. Patent and Trademark Off., Washington, D. C.
- Wang, C., and A. Mandelis (1999), Purely thermal-wave photopyroelectric interferometry, *J. Appl. Phys.*, *85*, 8366–8377.
- Yodh, A., and B. Chance (1995), Spectroscopy and imaging with diffusing light, *Phys. Today*, *48*, 34–40.
- Young, P. D., and C. S. Cox (1981), Electromagnetic active source sounding near the East Pacific Rise, *Geophys. Res. Lett.*, *8*, 1043–1046.
- Zhou, X., N. Chang, and S. Li (2009), Applications of SAR interferometry in Earth and environmental science research, *Sensors*, *9*, 1876–1912.

Y. Fan and R. Snieder, Center for Wave Phenomena, Colorado School of Mines, 1500 Illinois St., Golden, CO 80401, USA. (yfan@mymail.mines.edu)

J. Hunziker and E. Slob, Section of Applied Geophysics and Petrophysics, Department of Geotechnology, Delft University of Technology, Mijnbouwstraat 120, NL-2628 RX Delft, Netherlands.

M. Rosenquist, J. Sheiman, and J. Singer, Shell International Exploration and Production, PO Box 2463, Houston, TX 77025, USA.